Supplementary materials

Controllable synthesis of single-layer graphene over cobalt nanoparticles and insight into active sites for efficient oxygen evolution

Gisang Park,[a] Cheol-Hwan Shin,[a] Joonhee Kang,*[b] Kug-Seung Lee,*[c] Chunfei Zhang,[a] Byeonghwa Lim,[d] CheolGi Kim,[d] Jong-Sung Yu*[a]

a. Department of Energy Science and Engineering, Daegu Gyeongbuk Institute of Science & Technology (DGIST), Daegu, 42988, Republic of Korea.

b. Platform Technology Laboratory, Korea Institute of Energy Research, 71-2 Jang-dong, Yuseong-gu, Daejeon 305-343.

c. Pohang Accelerator Laboratory (PAL), Pohang University of Science and Technology (POSTECH), Pohang 790-784, South Korea.

d. Department of Emerging Materials Science, Daegu Gyeongbuk Institute of Science & Technology (DGIST), Daegu, 42988, Republic of Korea.

*Corresponding authors
E-mail:
j.kang@kier.re.kr
lks3006@postech.ac.kr
jsyu@dgist.ac.kr

Experimental

Magnetic field strength between the magnet and Co@N-SG particles

To calculate the holding force between the magnet and Co@N-SG particles, magnetic flux density (B) has calculated by using equation S7.

$$B = \mu 0\ M\frac{1}{2}\left(\frac{L-2z}{\sqrt{4R^2+(L-2z)^2}}+\frac{L+2z}{\sqrt{4R^2+(L+2z)^2}}\right)$$

Equation S7)

where R_{magnet}, L_{magnet}, z, μ_0 and M are the radius of the magnet, the height of the magnet, distance between Co@N-SG particle and the magnet, permeability in vacuum, and the molar mass of Co@N-SG particles, respectively. The particle size of 15.1 nm for Co@N-SG was used for this calculation.

For R_{magnet} = 5 mm, L_{magnet} = 2 mm, z = 0.8 mm, $\mu_0 = 4\pi\times10^{-7}$ H·m^{-1}, M = 811534.2 g·mol^{-1}, the magnetic flux density (B) is approximately 0.1930 T.

Material characterization

The X-ray diffraction (XRD) patterns were collected using a Rigaku Smartlab diffractometer with Cu K_α radiation using a Ni β-filter at a scan rate of 3 ° min^{-1}. The X-ray source was obtained at 40 kV and 30 mA. Scanning electron microscopy (SEM) images were obtained using a Hitachi S-4700 microscope operated at an acceleration voltage of 10 kV, and high-resolution transmission electron microscopy (HR-TEM) images were obtained using a HF3300 microscope operated at an acceleration voltage of 200 kV. Nitrogen adsorption-desorption isotherms were measured at -196 °C using a Micromeritics ASAP2020 system. Specific surface areas of the samples were determined by nitrogen adsorption data using Brunauer-Emmett-Teller (BET) equation. X-ray photoelectron spectroscopy (XPS) analyses were performed with an AXIS-NOVA (Kratos) X-ray photoelectron spectrometer, using a monochromated Al K_α X-ray source (hν = 1486.6 eV) operated at 150 W under a base pressure of 2.6 x 10^{-9} Torr. Raman spectroscopy measurements (Renishaw) were recorded using an Ar ion laser (λ = 514.5 nm).

X-ray absorption analysis

X-ray absorption fine structure (XAFS) was measured at 8C nano-probe XAFS beamline (BL8C) of Pohang Light Source (PLS-II) in the 3.0 GeV storage ring with a ring current of 250 mA. The X-ray beam was monochromated by a Si(111) double crystal where the beam intensity was reduced by 30 % to eliminate the higher-order harmonics. The X-ray beam was then delivered to a secondary source aperture where the beam size was adjusted to be 0.5 mm (v) × 1 mm (h). XAFS spectra were collected in both transmission and fluorescence modes. The obtained spectra were processed using Demeter package.

Defect analysis

Prior to the calculation, two important assumptions are established; 1) bare Co NPs has 100 % carbon defect and 2) defect-free Co@SG has 0 % defect. To obtain the fraction of exposed surface, the first oxidation peak area of each sample (I) in Fig. 4e is divided by the oxidation peak area (I_{Co}) of bare Co NP sample. Then, the obtained ratio is divided by corresponding BET surface area (S_{BET}) to obtain the exposed Co factor per unit surface area (unit is g m^{-2}) of each sample. Finally, the factor is divided by the factor of Co NPs to get a normalized value. Since the S_{BET} of Co@SG and Co@N-SG includes contribution from graphene shell as well as exposed Co surface, the S_{BET} is overestimated only for the exposed Co surface and thus the normalized value indicates the minimum defective fraction of the sample.

Electrochemical characterization

Electrochemical analysis of oxygen evolution reaction (OER) was carried out on a VSP potentiostat (Bio-Logic SAS) with a standard three-electrode cell composition in a 1.0 M KOH (pH = 13.8). An Ag/AgCl electrode was used as a

reference, and Pt wire was used as a counter electrode for electrochemical characterization. Hg/HgO electrode was used as a reference particularly for long-term stability test. Glassy carbon electrode (GCE) coated with each catalyst ink was used as a working electrode. The GCE was washed with Milli-Q water and ethanol to maintain the clean electrode surface before and after catalyst measurement. The potential conversion from Ag/AgCl or Hg/HgO to reversible hydrogen electrode (RHE) was performed according to Equation S1 and S2 below, respectively. Before measuring electrochemical OER performance, cycle voltammetry (CV) was carried out 5 times as a stabilization step. Linear sweep voltammetry (LSV) and CV were performed with a scan rate of 20 mV s^{-1}. 85 % iR compensation was adopted for the obtained LSV curves according to Equation S3. A Tafel plot was calculated from the corresponding LSV curve by Equation S4. Chronopotentiometric measurement was performed as a function of time at a fixed current density. Electrochemical impedance spectrum (EIS) was measured with an AC voltage amplitude of 10 mV in a frequency range of 1.0×10^2 - 2.0×10^6 Hz.

1.0 M KOH electrolyte containing 10 mM KCN was prepared to perform cyanide poisoning experiment for Co@G samples.

Equation S1

$E(RHE) = E_0(Ag/AgCl, sat.\ KCl) + 0.059 \times pH + E_{applied}$

where $E_0(Ag/AgCl, sat.\ KCl) = 0.197$ V (RHE)

Equation S2

$E(RHE) = E_0\ (Hg/HgO, 1.0\ M\ KOH) + 0.059 \times pH + E_{applied}$

where $E_0\ (Hg/HgO, 1.0\ M\ KOH) = 0.118$ V (RHE)

Equation S3

$E(RHE, iR\ compensation) = E(RHE) - iR \times 0.85$

where E(RHE) is applied potential vs RHE, i is the recorded current, and R is the solution resistance measured by EIS.

Equation S4

$$\eta = b \cdot log(j/j_0)$$

where η is the overpotential, b is the Tafel slope, j is the current density, and j_0 is the exchange current density.

Determination of generated oxygen

The amount of generated O_2 was analyzed every 20 minutes by using a Bruker 450 GC online gas chromatograph. The first 60 minutes were spent to reach the equilibrium state of O_2 and N_2 flow and then the measurement was started (200 sccm N_2 flow condition was used for carrying produced O_2 gas). Electrochemical measurements were performed on the VSP electrochemical workstation (Bio-Logic SAS) with a three-electrode setup in 100 mL, 1.0 M KOH aqueous solution. The yield of generated oxygen(η_{O2}) was determined by the equation below.

Equation S5

$$n_{O2} = \frac{I \times t}{z \times F}$$

where n_{O2} is the number of mol O_2 generated, I is current (A), t is time (s), z is the transfer of electron (for O_2, z = 4), and F is Faraday constant (96500 C mol^{-1}).

Computational details

All structural minimization and free energy calculations were performed using Vienna *ab-initio* simulation package (VASP).[1] A generalized gradient approximation was used with Perdew-Burke-Ernzerhof exchange-correlation

functionals and a projector augmented wave was used to generate core electron pseudo-potentials.[2,3] Cutoff energy was 500 eV and a Monkhorst-Pack 3x3x1 *k*-points scheme was applied to integrate the Brillouin zone. Each calculation was continued until the forces acting on all atoms were less than 0.02 eV $Å^{-1}$ with the energy convergence criterion of 10^{-5} eV. DFT-D3 method of Grimme was employed to consider van der Waals interactions.[4] Three models of *fcc* Co (111) with graphene structure were considered: TOP-FCC, TOP-HCP and FCC-HCP. Among them, the TOP-FCC was shown to be the most stable structure.

In an alkaline medium, the OER could occur via a four-electron reaction pathway:

Equation S6

$$* + 4OH^- \rightarrow OH^* + 3OH^- + e^-$$
$$\rightarrow O^* + H_2O + 2OH^- + 2e^-$$
$$\rightarrow OOH^* + H_2O + OH^- + 3e^-$$
$$\rightarrow O_2 + 2H_2O + 4e^-$$

The adsorption free energies (ΔG) of the intermediates were obtained according to Equation S7, $\Delta G = \Delta E + \Delta ZPE - T\Delta S + eU$, where ΔE, ΔZPE, T, ΔS and eU are the adsorption energy from DFT calculations, the zero-point vibration energy, temperature (298 K), entropy, and applied potential, respectively. The values of $\Delta ZPE - T\Delta S$ = 0.30, 0.05 and 0.32 eV (for OH*, O*, and OOH* reaction) were used for correction.[5]

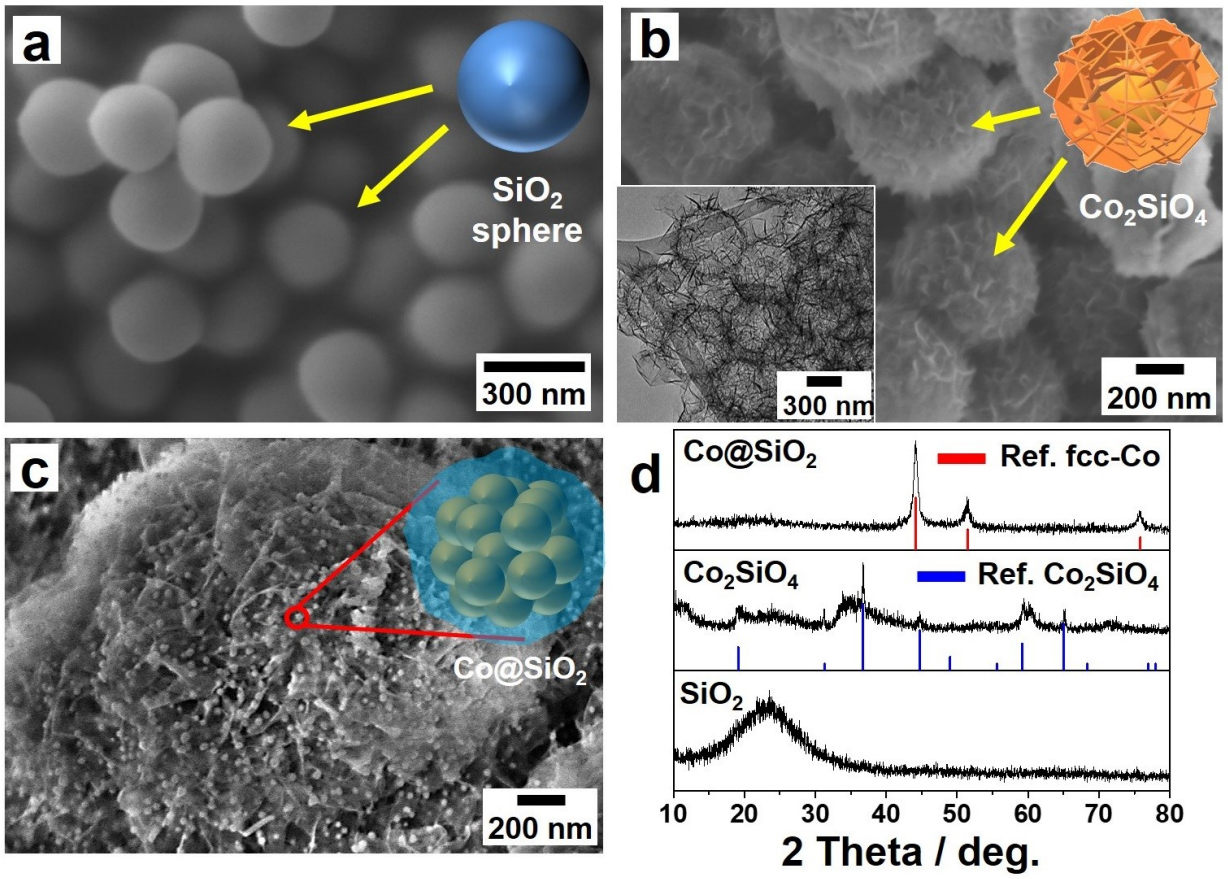

Fig. S1 Structure characterization of SiO_2 spheres, cobalt silicate (Co_2SiO_4) and $Co@SiO_2$. SEM images of a) SiO_2 spheres, b) Co_2SiO_4 produced after hydrothermal reaction, and c) individual Co NPs embedded in SiO_2 frameworks ($Co@SiO_2$) generated after reduction under H_2/Ar gas flow. d) Corresponding XRD patterns of the products produced in each synthesis step. (Ref. fcc-Co: JCPDS 15-0806 and Ref. Co_2SiO_4: cobalt silicate series, JCPDS 21-0872).

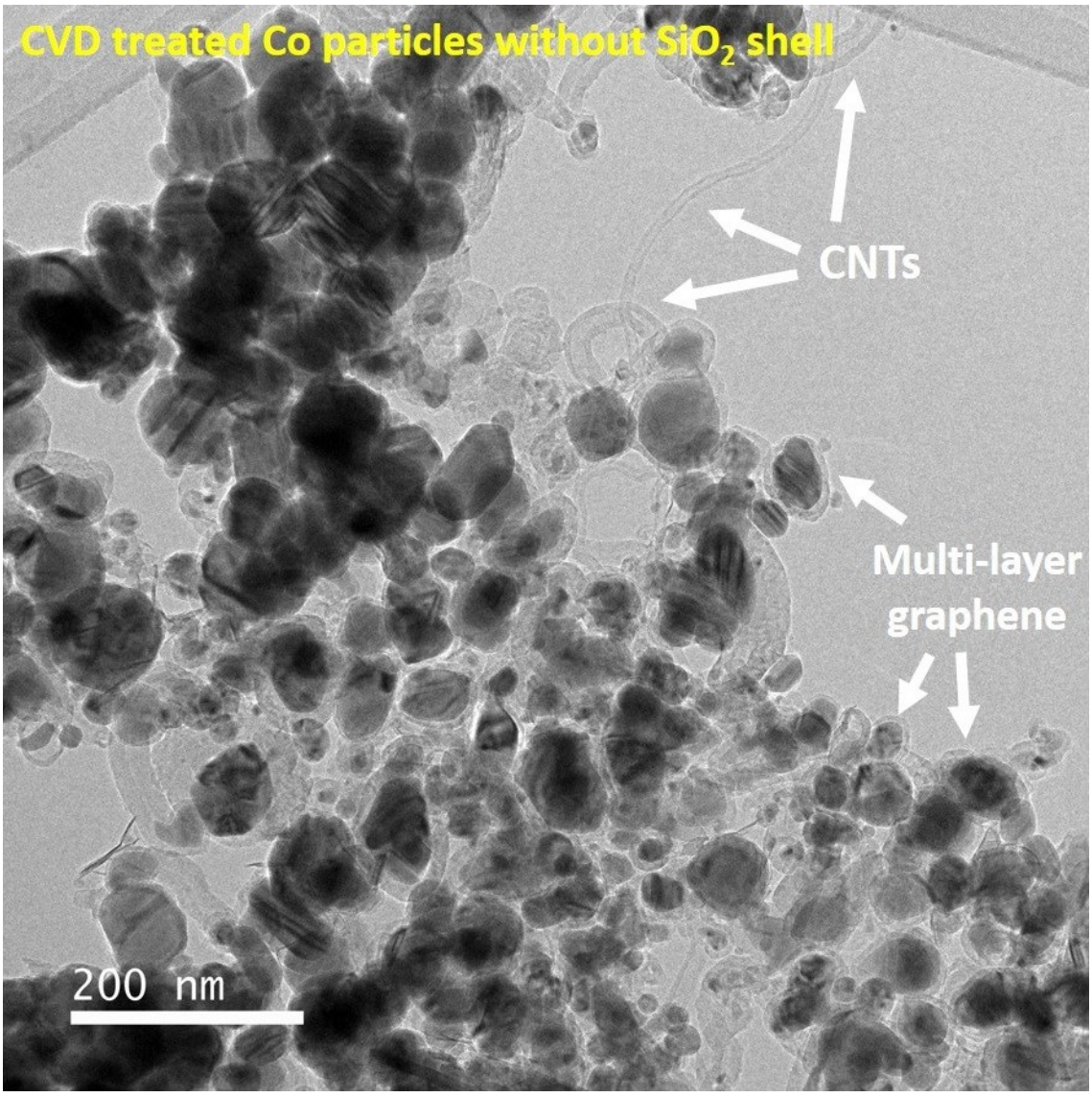

Fig. S2 TEM image of Co particles after CVD treatment for 10 min without SiO_2 coating under the identical CVD conditions. Particles are easily agglomerated, and excessive growth of CNTs and multi-layer graphene shell is observed.

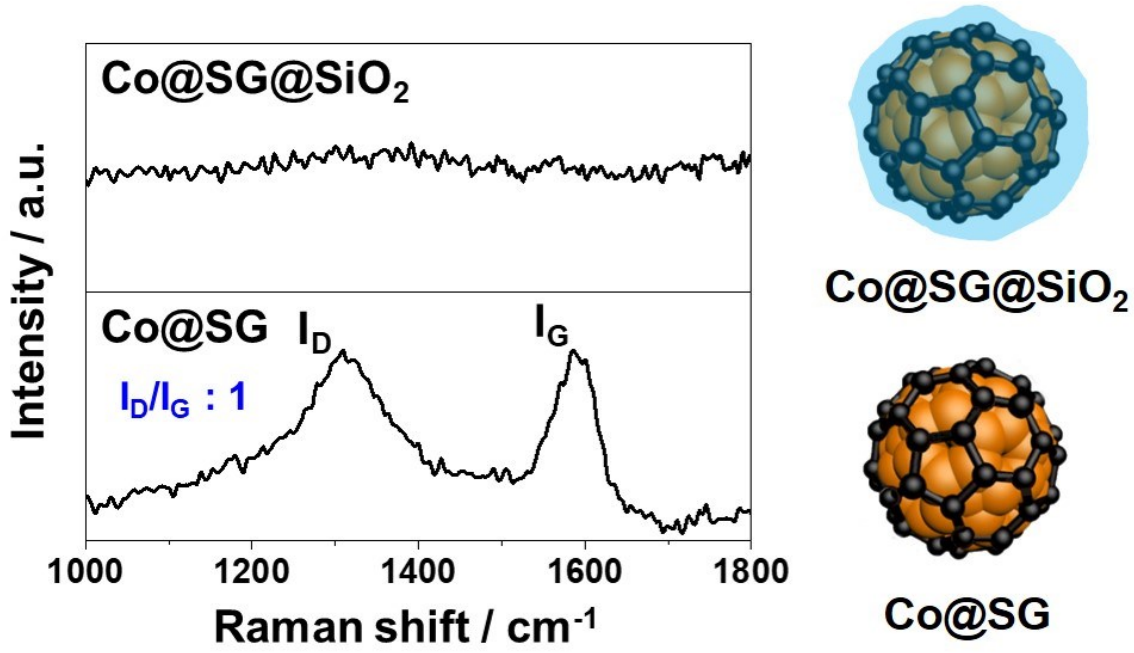

Fig. S3 Raman spectra of Co@SG@SiO_2 and Co@SG. The Co@SG@SiO_2 shows no Raman signals, whereas silica-free Co@SG displays the characteristic carbon signals at 1319 and 1587 cm^{-1}.

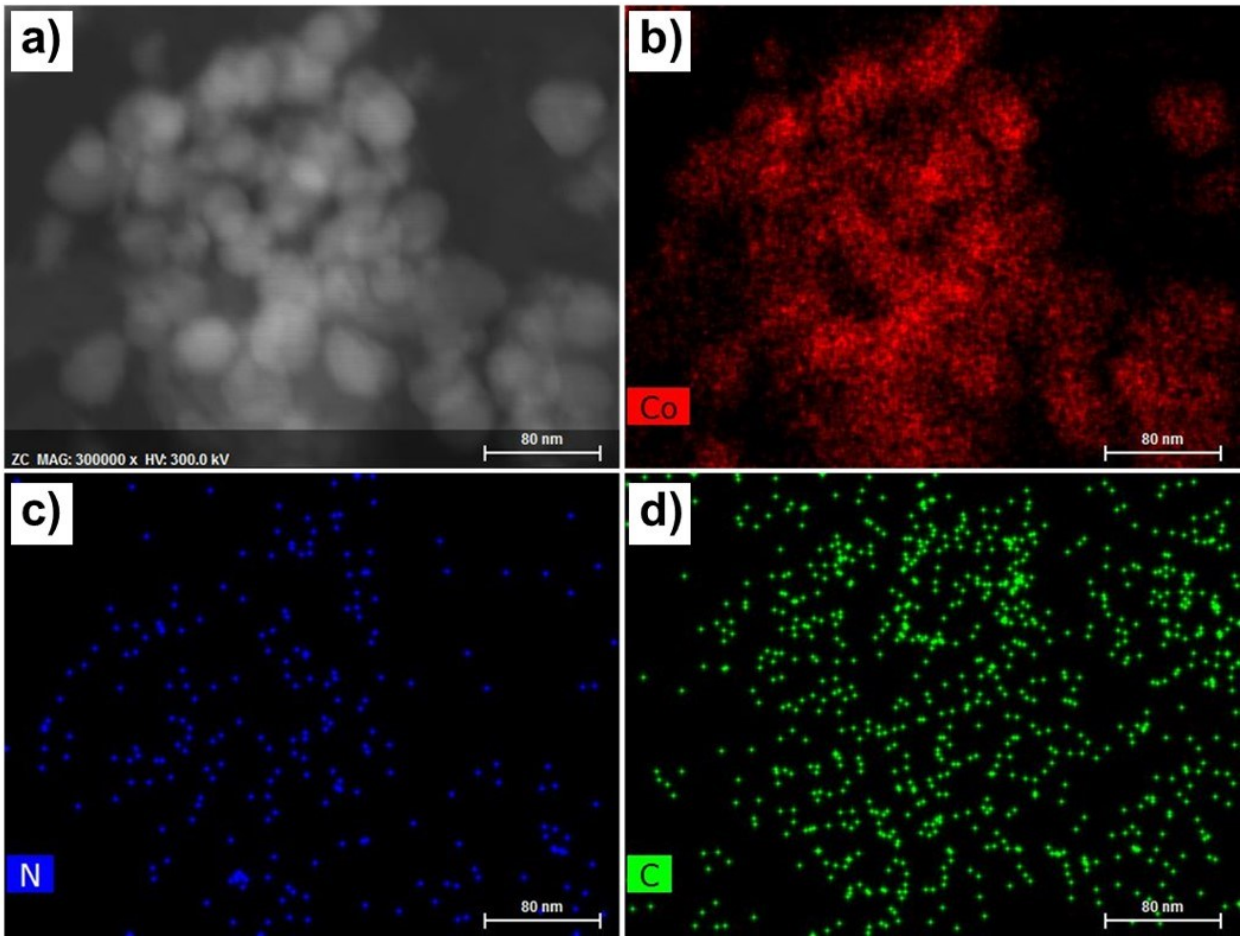

Fig. S4 EDS mapping data for Co@N-SG. a) STEM image. b), c), and d) Elemental mappings for Co, N, and C, respectively.

Low intensity signals are observed for C and N because of the very thin single-layer graphene compared to high intensity signal for Co.

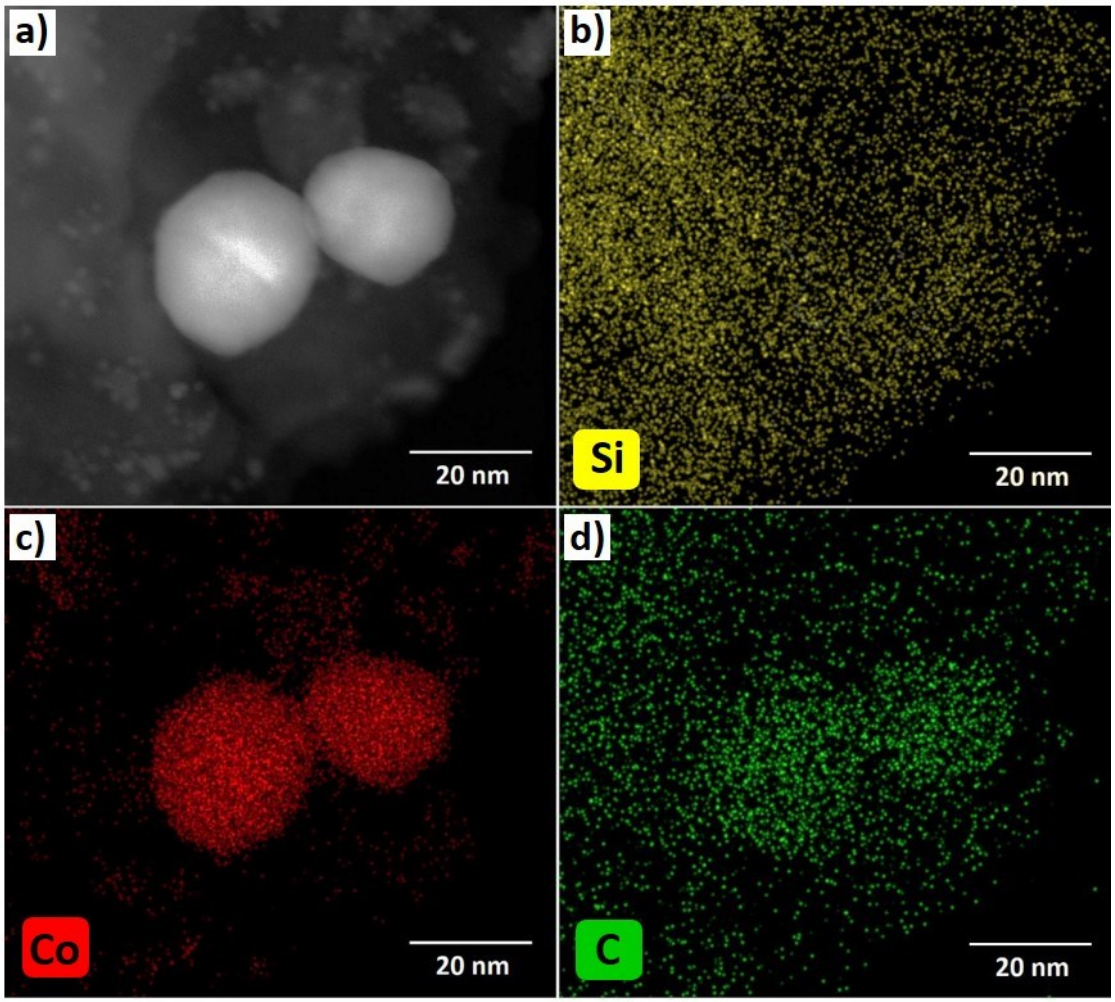

Fig. S5 EDS mapping data for Co@N-SG@SiO_2 structure. a) STEM image. b), c), and d) Elemental mappings for Si, Co, and C, respectively.

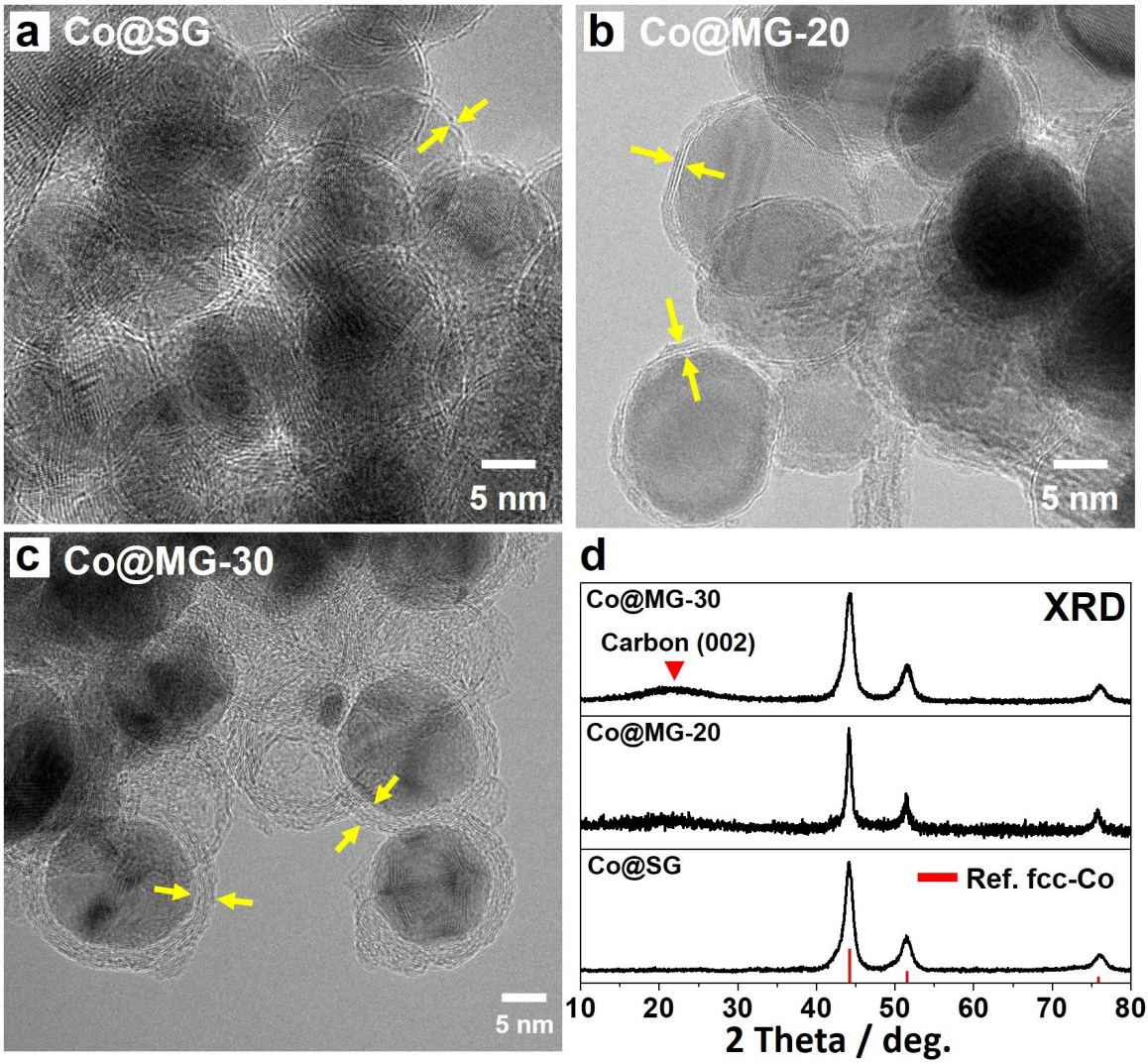

Fig. S6 HR-TEM images and XRD patterns of Co@G samples. HR-TEM images of a) Co@SG, b) Co@MG-20 and c) Co@MG-30, and d) corresponding XRD patterns for the samples prepared by 10, 20, and 30 min exposure to C_2H_2 gas.

This proves the possibility of controlling the graphene shell layers including selective growth of single-layer graphene in Co@SG. The (002) signal is usually observed for CNTs, multi-layer graphene and amorphous carbon materials.

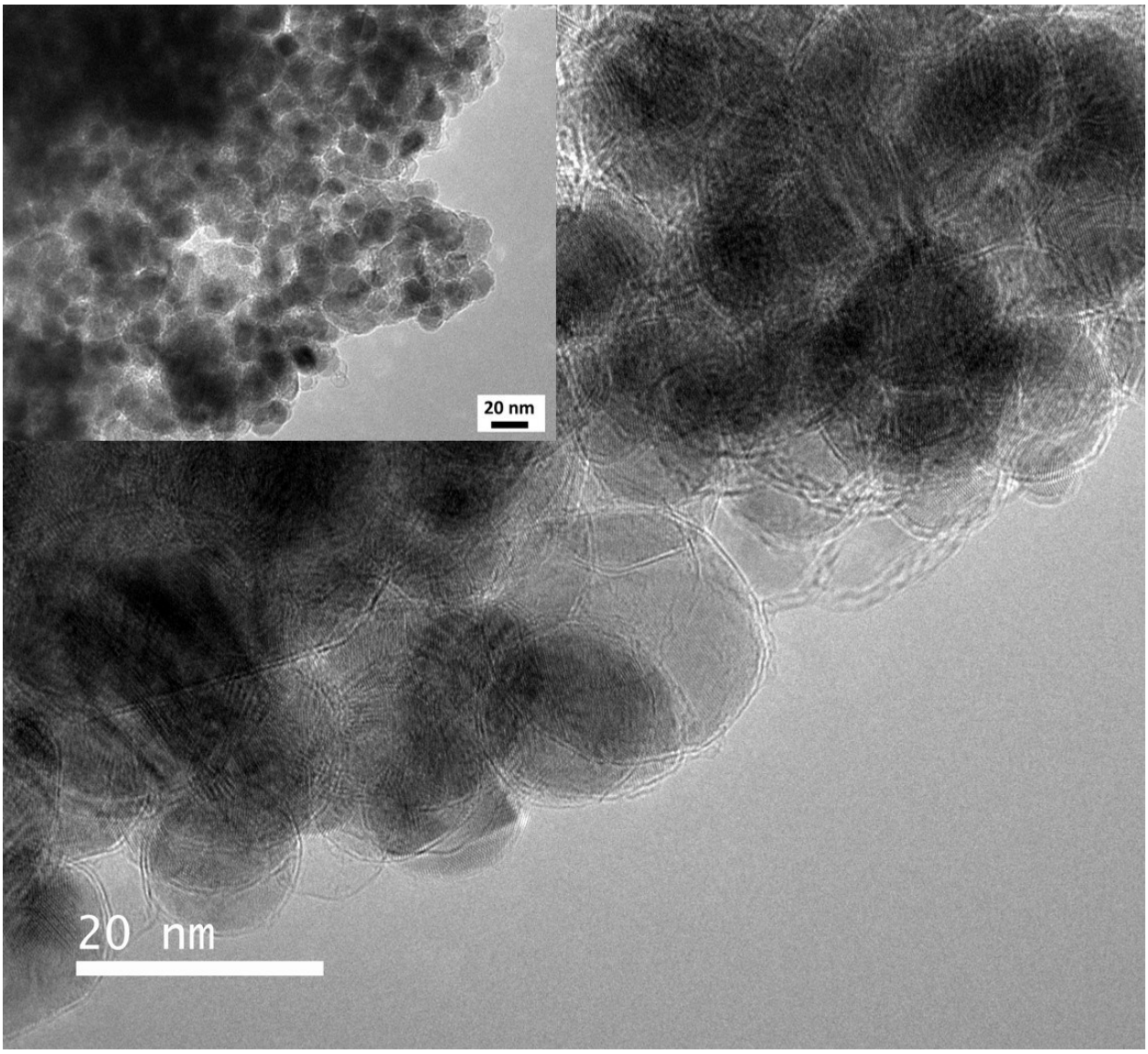

Fig. S7 TEM image of Co@N-SG. Inset shows the corresponding TEM image of the Co@N-SG sample at low magnification.

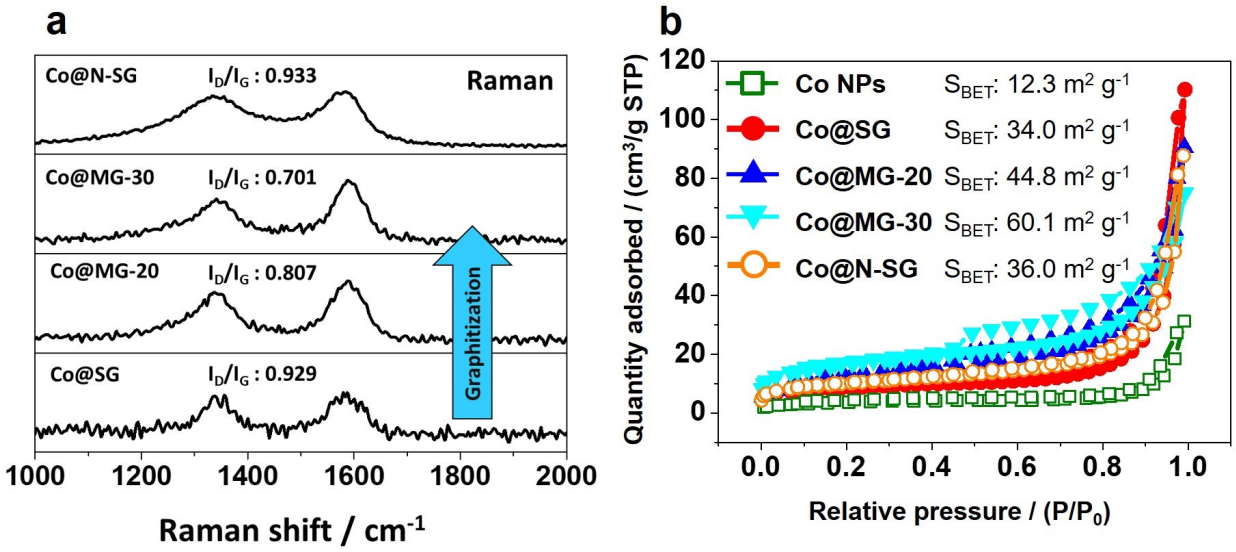

Fig. S8 Raman and surface area measurements. a) Raman spectra for Co@SG, Co@MG-20, and Co@MG-30 samples prepared by 10, 20, and 30 min exposure to C_2H_2 gas. Co@N-SG sample was prepared by 10 min exposure to C_2H_2 and NH_3 gas. b) Nitrogen adsorption-desorption isotherms of Co NPs, Co@SG, Co@MG-20, Co@MG-30 and Co@N-SG with respective BET surface area.

As the number of graphene layers increases, the BET surface area increases due to the increase of the carbon ratio in the graphene-coated Co (Co@G) samples.

Table S1 ICP-OES analysis of Co@SG, Co@MG-20, Co@MG-30, and Co@N-SG. Each sample was dissolved in 3.0 M HCl solution and then diluted 100 times to make 10 ppm solution of each sample.

Sample	Element	Co (wt %)
Co@SG	Co	86.44
Co@MG-20	Co	70.08
Co@MG-30	Co	48.32
Co@N-SG	Co	85.52
Matrix solution	Co	0

Table S2 Element analysis of Co@SG, Co@MG-20, Co@MG-30, and Co@N-SG.

Sample	C (wt %)	H (wt %)	N (wt %)
Co@SG	10.31	0.468	0
Co@MG-20	26.01	0.257	0
Co@MG-30	43.85	0.601	0
Co@N-SG	12.29	1.068	0.51

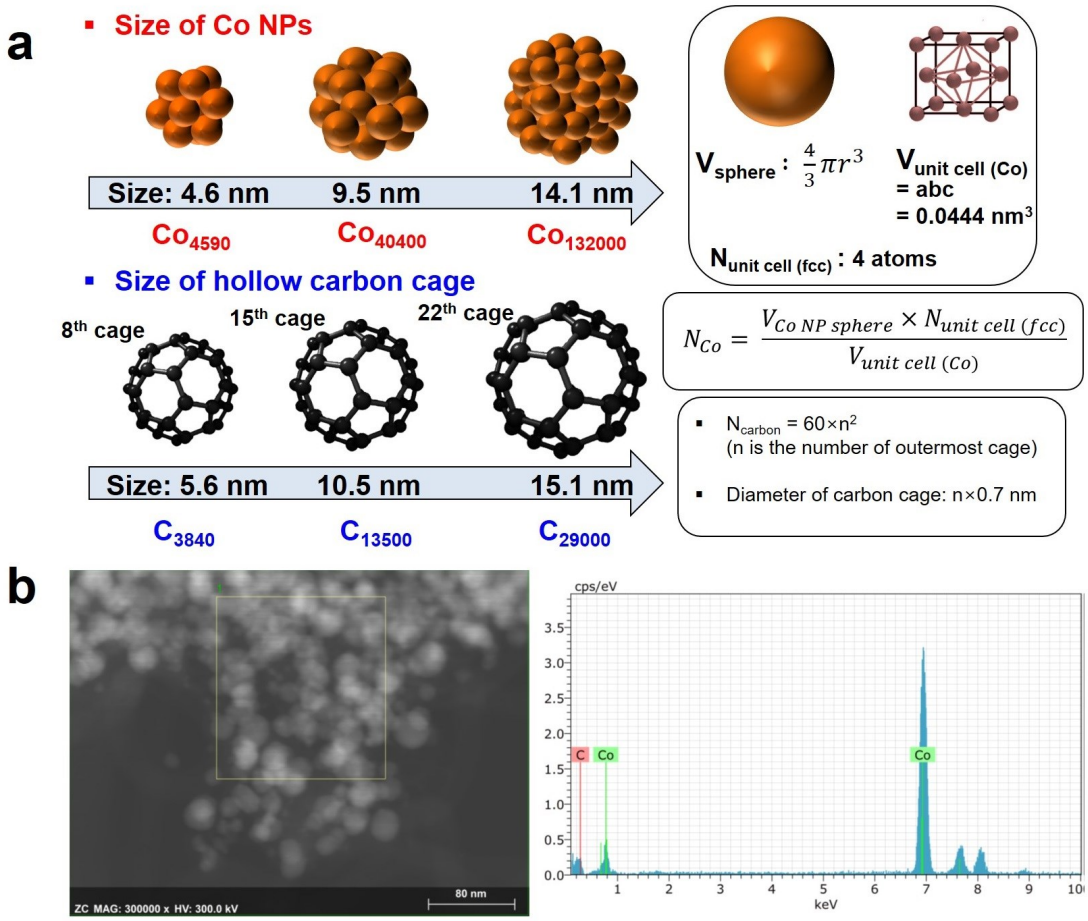

Spectrum: 1

El	AN	Series	unn. C [wt.%]	norm. C [wt.%]	Atom. C [at.%]	Error (1 Sigma) [wt.%]
Co	27	K-series	94.46	94.46	77.66	3.07
C	6	K-series	5.54	5.54	22.34	0.45
Total:			100.00	100.00	100.00	

Fig. S9 Calculation of Co:C ratio and EDS spectrum of Co@SG. a) In the calculation of the Co:C ratio, the fcc Co NP is presumed to have a perfect sphere with unit cell volume of 0.0444 nm^3. The carbon cage is presumed to be composed of sp^2 carbon only, where C_6 ring is not drown in proper scale. The number of carbon atoms in a single layer sp^2 carbon shell can be estimated by the equation of $N_{carbon}=60n^2$.[6] b) EDS spectrum of Co@SG. The amount of carbon is approximately 5 - 6 wt %.

The experimentally determined contents of Co and C are about 86, 70, 48 wt.% and 10, 26, 43 wt.% for Co@SG, Co@MG-20 and Co@MG-30, respectively. The total content of both Co and C was found to be less than 100 % probably because of some loss of the sample including the partial oxidation of Co NPs and some impurities (Table S3).

Table S3 Comparison of theoretical calculation and experimental results of M:C weight ratio in various M@G samples.

Sample	Ref.	Analysis method	Particle size	M : C weight ratio
Fcc*-Co@SG	This work	Calculation	15.1 nm	96 : 4
Fcc*-Co@DG**	This work	Calculation	15.1 nm	91 : 9
Fcc*-Co@SG	This work	Calculation	10 nm	93 : 7
Fcc*-Co@DG**	This work	Calculation	10 nm	85 : 15
Co@SG	**This work**	**ICP-OES and EA**	**10 - 15 nm**	**86 : 10**
Co@SG	**This work**	**EDS**	**10 - 15 nm**	**94 : 6**
Cr^{6+}@G	7	EELS**	Not measured	61 : 22
Fe@SG/CNT	8	XPS	2.6 nm	5.6 : 82
Co@G	9	ICP-OES, EA	6 – 10 nm	34 : 59
Co@NC	10	EA	30 – 50 nm	Not measured (28 wt.% C)

Abbreviations. Fcc*: face-centered cubic, EELS**: electron energy loss spectroscopy, and DG**: double-layer graphene shell.

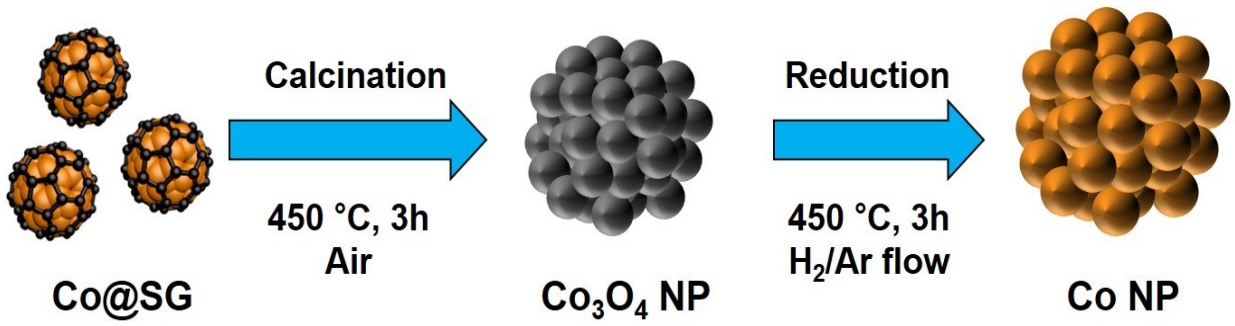

Scheme S1 Schematic presentation of preparation of bare Co NPs. Graphene shell in Co@SG is removed by oxidative pyrolysis through the calcination in air, and the resulting carbon-free oxidized Co NPs are reduced in H_2/Ar flow to give bare metallic Co NPs.

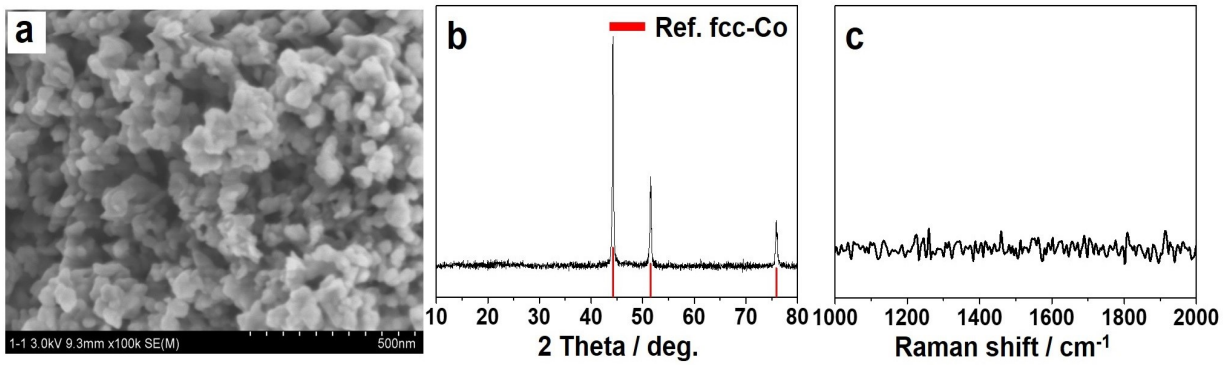

Fig. S10 Characterization of as-prepared bare Co NPs. a) SEM image, b) XRD pattern and c) Raman spectrum of the bare Co NPs prepared according to scheme S1. Red vertical lines correspond to the XRD peak positions of fcc-cobalt (JCPDS 15-0806).

The average particle size of the Co NPs increases to 36.6 ± 5.6 nm due to thermal agglomeration of initial Co NPs in Co@SG with particle size of 15 nm ± 3.0 nm. Graphene's D- and G-bands disappear in Raman spectrum of the as-prepared bare Co NPs.

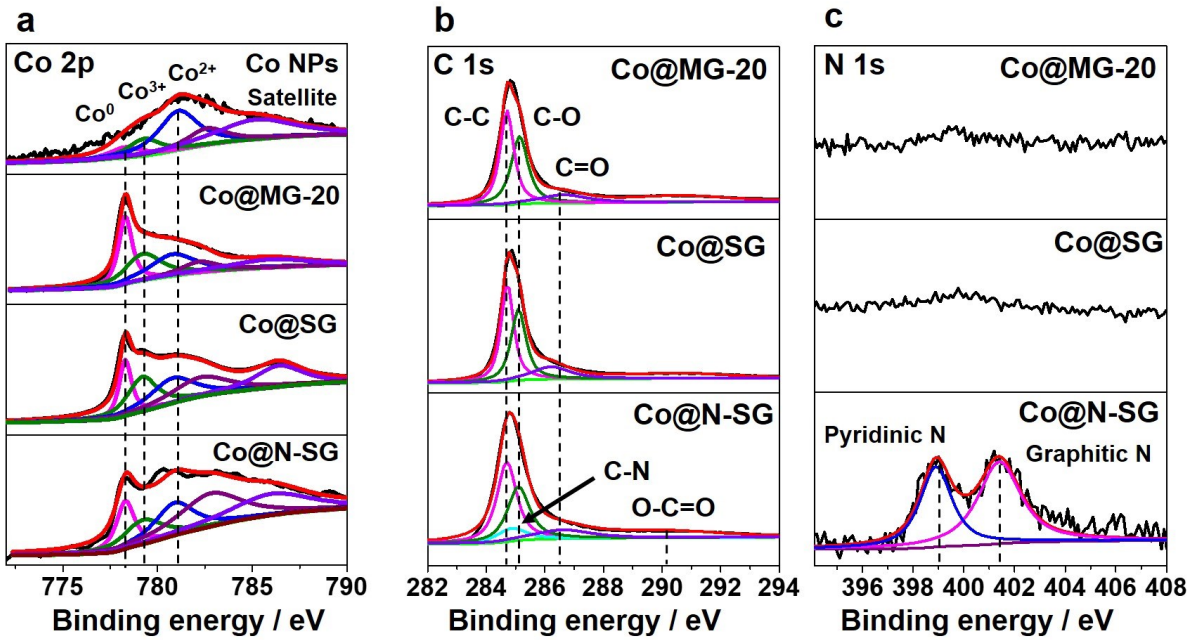

Fig. S11 XPS data for Co@G samples. a) high resolution Co 2p spectra, b) C 1s spectra and c) N 1s spectra of Co@N-SG, Co@SG, and Co@MG-20**.**

Peaks at around 783 and 786 eV are assigned to plasmon loss and shake-up satellite, respectively. Since the surface of bare Co particles is not protected from oxidation, cationic Co^{3+} and Co^{2+} are mainly observed with little metallic Co.

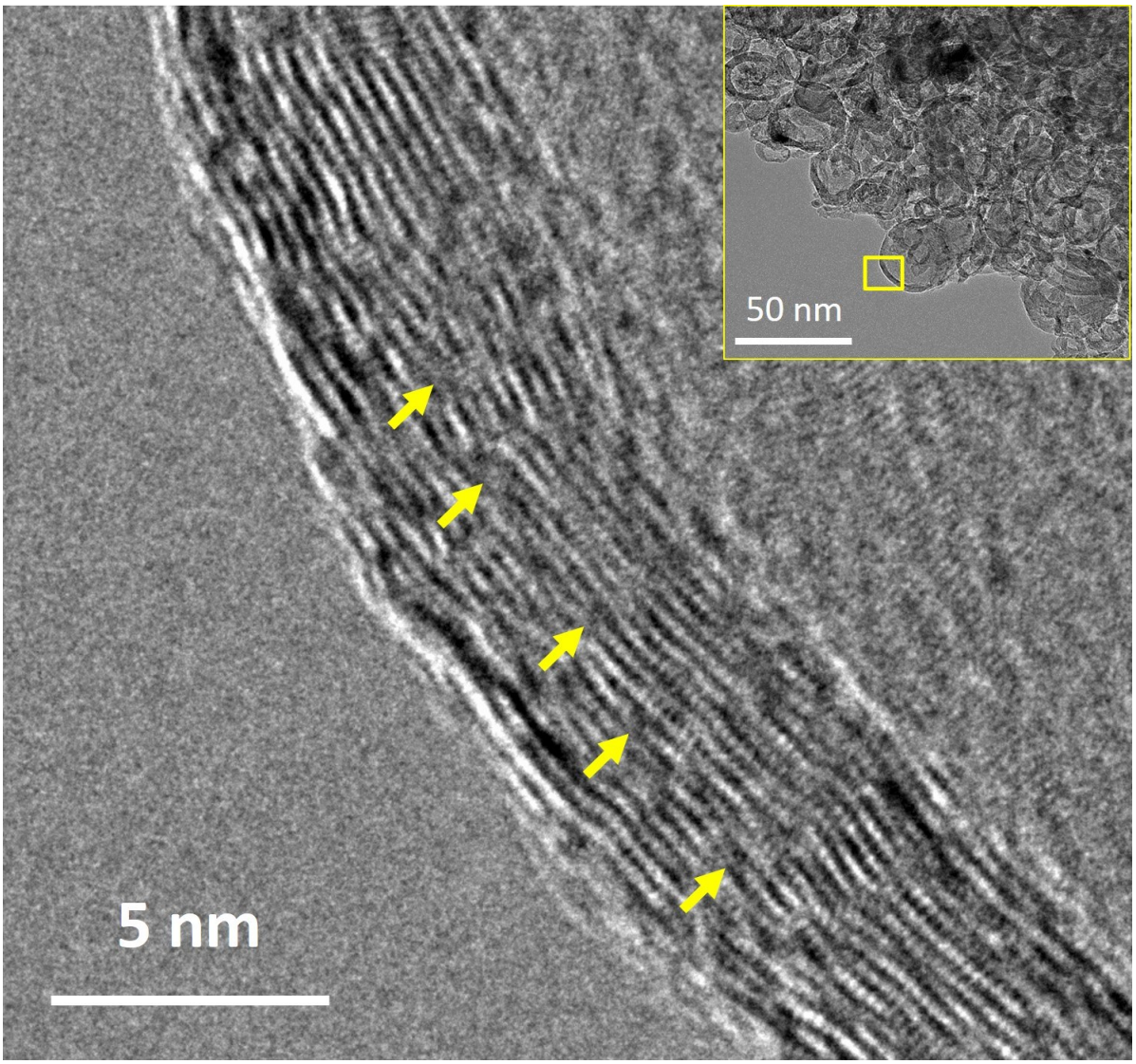

Fig. S12 TEM images of hollow multi-layer graphene cages. The cages are obtained by HF treatment of Co@MG-30 for 5 days. Yellow arrows indicate discontinuous carbon lattice, which may be related to carbon defects. Inset shows the corresponding TEM image of the hollow multi-layer graphene cages at low magnification

Even though the core is covered by thick multiple graphene layer, acid molecules can still penetrate the shell through defect vacancies to dissolve the core metal.

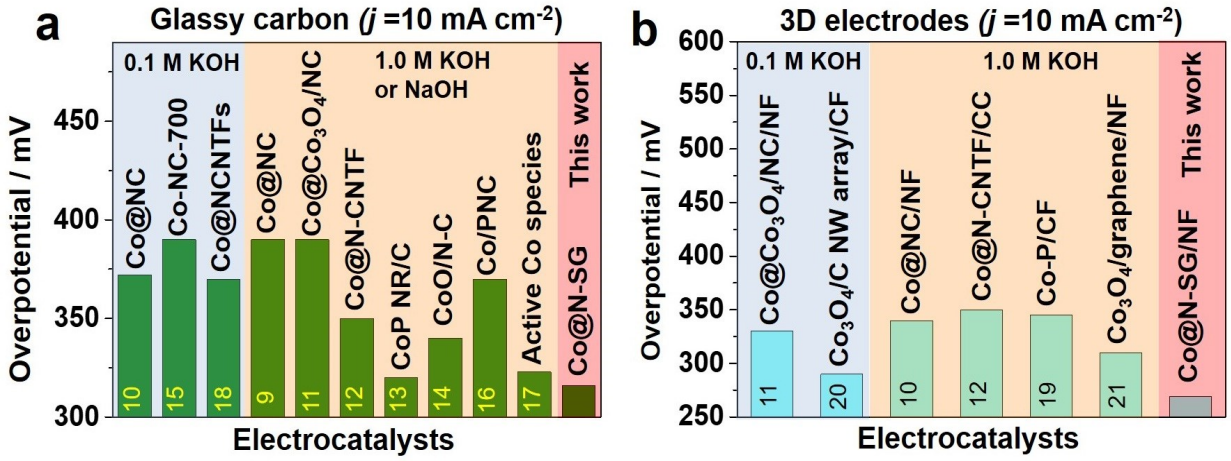

Fig. S13 The comparison of OER overpotentials for Co-based catalysts. The overpotentials measured a) on glassy carbon electrode and b) on 3D electrodes at a current density of 10 mA cm^{-2} for Co@N-SG and other Co-based catalysts in the literature. (NF: Ni foam, CF: copper foam, CC: carbon cloth). The numbers in the bottom of the bars indicate reference numbers.

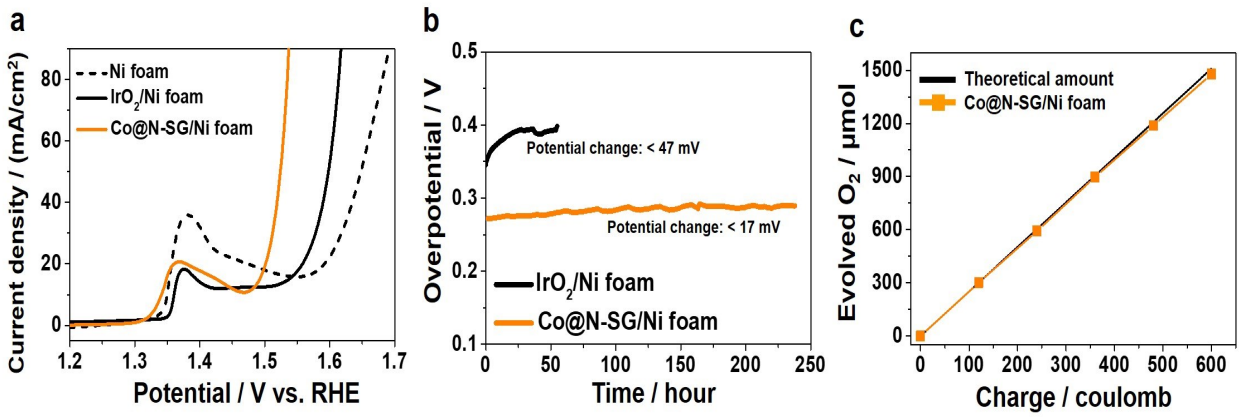

Fig. S14 OER activity, stability and O_2 evolution tests. a) LSV curves and b) chronopotentiometry tests for IrO_2 and Co@N-SG loaded on Ni foam electrode at 10 mA cm^{-2} for 240 h. c) Comparison of experimental and theoretical amounts of generated O_2 on Co@N-SG/Ni foam electrode.

Table S4 OER performances for various carbon-decorated Co-based catalysts on glassy carbon electrode.

Material	**Electrolyte**	**Overpotential (at 10 mA cm^{-2})**	**Mass loading (mg cm^{-2})**	**Reference**
Co@NC	1.0 M NaOH	390 mV	0.320	9
Co@NC	0.1 M KOH	372 mV	0.560	10
Co@Co_3O_4/NC	1.0 M KOH	390 mV	0.210	11
Co@N-CNTF	1.0 M KOH	350 mV	0.280	12
CoP NR/C	1.0 M KOH	320 mV	0.710	13
CoO/N-C	1.0 M KOH	340 mV	0.708	14
Co-NC-700	0.1 M KOH	390 mV	0.240	15
Co/PNC	1.0 M KOH	370 mV	0.354	16
Active Co species	1.0 M KOH	323 mV	0.466	17
Co@NCNTFs	0.1 M KOH	370 mV	0.200	18
Co@N-SG	**1.0 M KOH**	**316 mV**	**0.142**	**This work**

Table S5 OER performances for Co catalysts loaded on different 3D electrodes**.**

Material	Electrolyte	Overpotential (at 10 mA cm^{-2})	Mass loading (mg cm^{-2})	Reference
Co@NC/Ni foam	1.0 M KOH	340 mV	0.5	10
Co@Co_3O_4/NC/Ni foam	0.1M KOH	330 mV	-	11
Co@N-CNTF/carbon cloth	1.0 M KOH	350 mV	1.0	12
Co-P/Cu foil	1.0 M KOH	345 mV	-	19
Co_3O_4/C NW array/Cu foil	0.1 M KOH	290 mV	0.2	20
Co_3O_4/graphene/Ni foam	1.0 M KOH	310 mV	1.0	21
Co@N-SG/Ni foam	**1.0 M KOH**	**269 mV**	**0.4**	**This work**

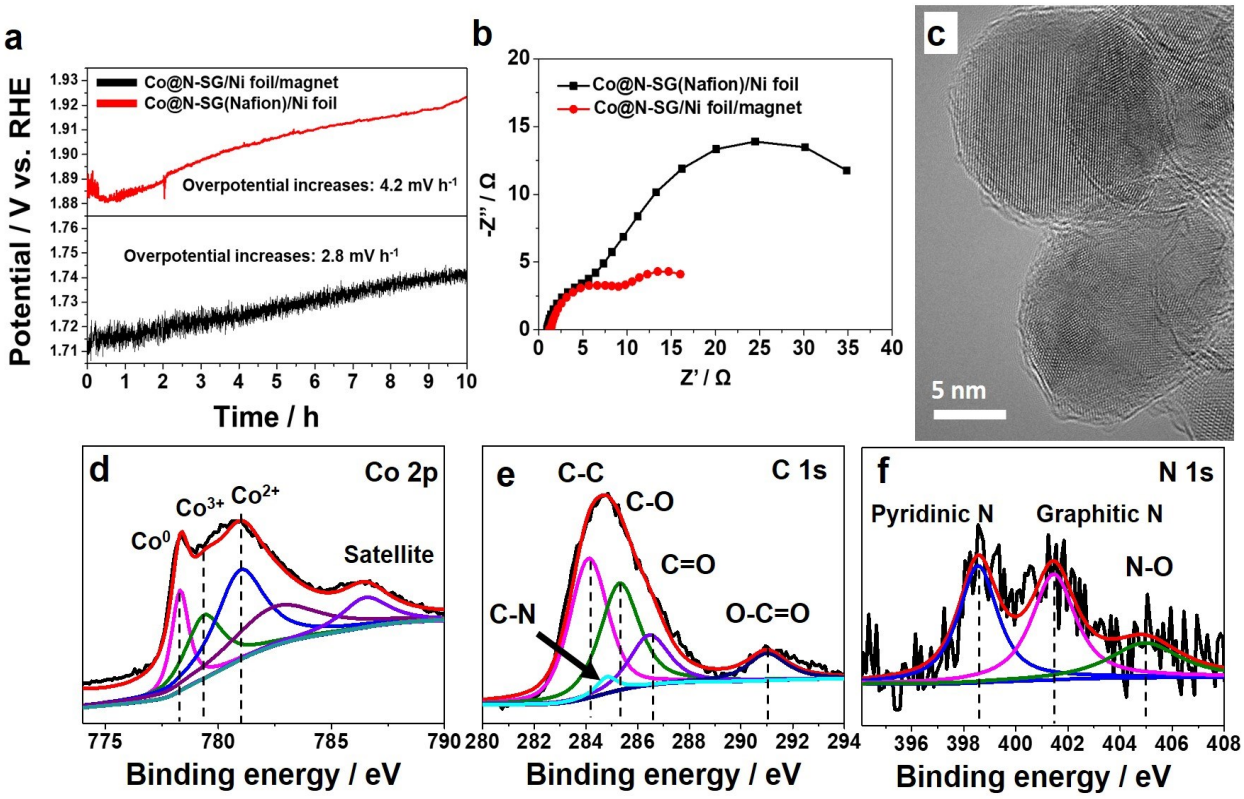

Fig. S15 Chronopotentiometry analysis for OER. a) Chronopotentiometry data for Co@N-SG/Ni foil/magnet and Co@N-SG/Ni foil/Nafion electrodes. The potential was measured at a current density of 100 mA cm^{-2} for 10 h. b) Nyquist plots for Co@N-SG(Nafion)/Ni foil and Co@N-SG/Ni foil/magnet electrodes at 1.53 V vs. RHE. The first smaller semicircle corresponds to charge transfer for oxidation of Ni^{2+}, while the larger semicircle to charge transfer arising from OER. c) TEM image after stability test for 10 h. d-f) XPS spectra of Co@N-SG after the chronopotentiometry test for 10 h.

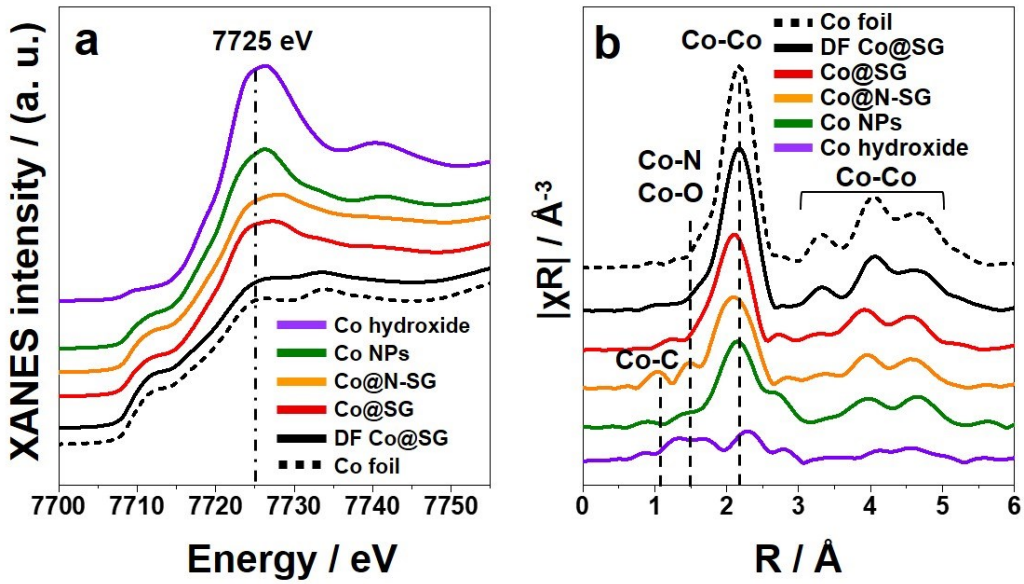

Fig. S16 X-ray absorption analysis for Co samples. a) Co K-edge XANES and b) Co K-edge FT-EXAFS.

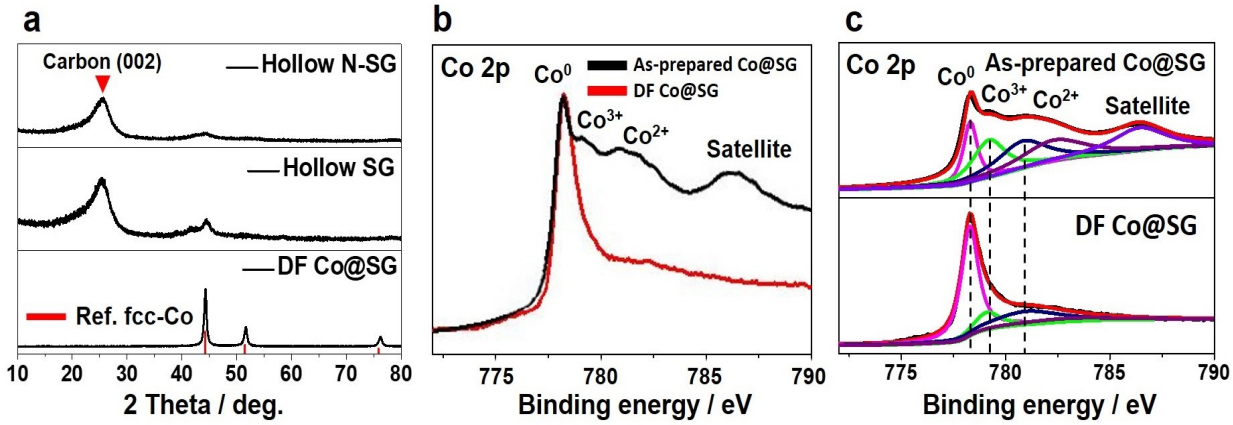

Fig. S17 XRD and XPS analysis of samples. a) XRD patterns of DF Co@SG particles, hollow SG and N-SG cages. b) Comparison of Co 2p XPS for as-prepared Co@SG and DF Co@SG. c) Co 2p XPS of as-prepared Co@SG and DF Co@SG with deconvolution.

The purified hollow N-SG and SG carbon cages show a broad peak near at 26 °, typical of carbon (002), indicating that small amount of multi-layer graphene shell impurities exists in these core-shell samples. Or some single layer graphene shells may self-interact or interact with other single layer shells to form a multi-layered shell during acid treatment.

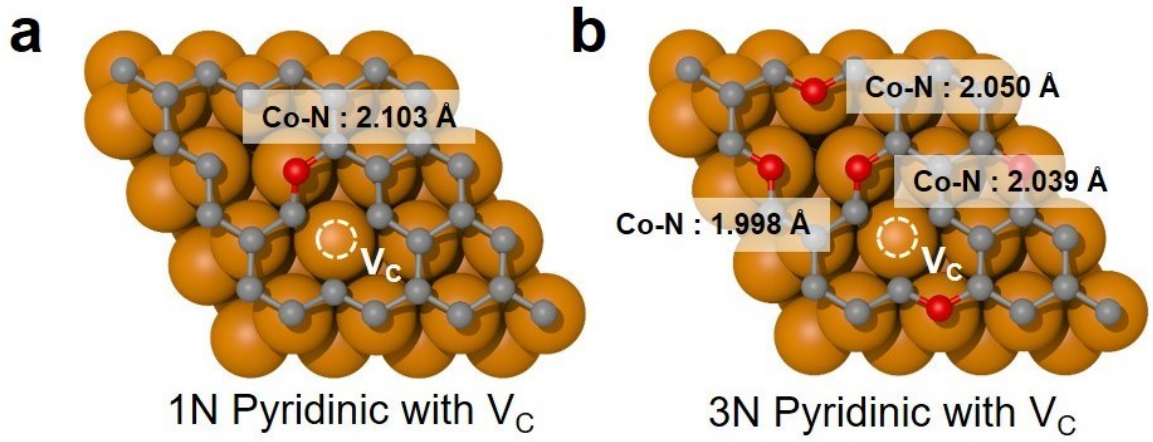

Fig. S18 a) Calculated Co-N bond distances for model systems of Co@N-SG (1N and 3N pyridinic with a carbon vacancy site). The orange, gray, and red spheres denote Co, C, and N atoms, respectively. The average Co-N bond distances was similar for both systems.

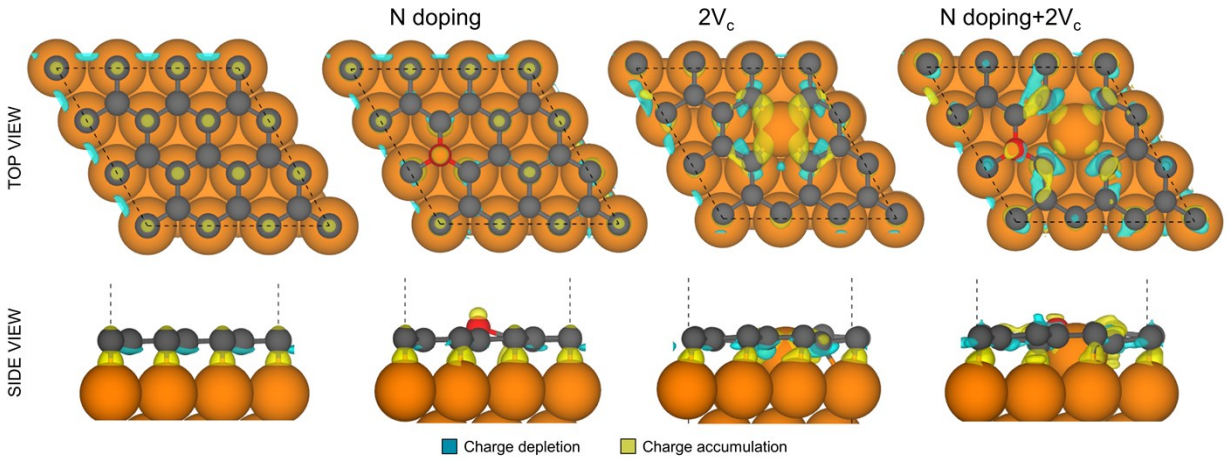

Fig. S19 The model systems and atomic charge density distributions of Co@SG, Co@N-SG (graphitic N), Co@SG (carbon defects; $2V_C$), and Co@N-SG (graphitic N with $2V_C$). The presence of carbon defect especially with N-doping highly affects to charge density of graphene in Co@SG.

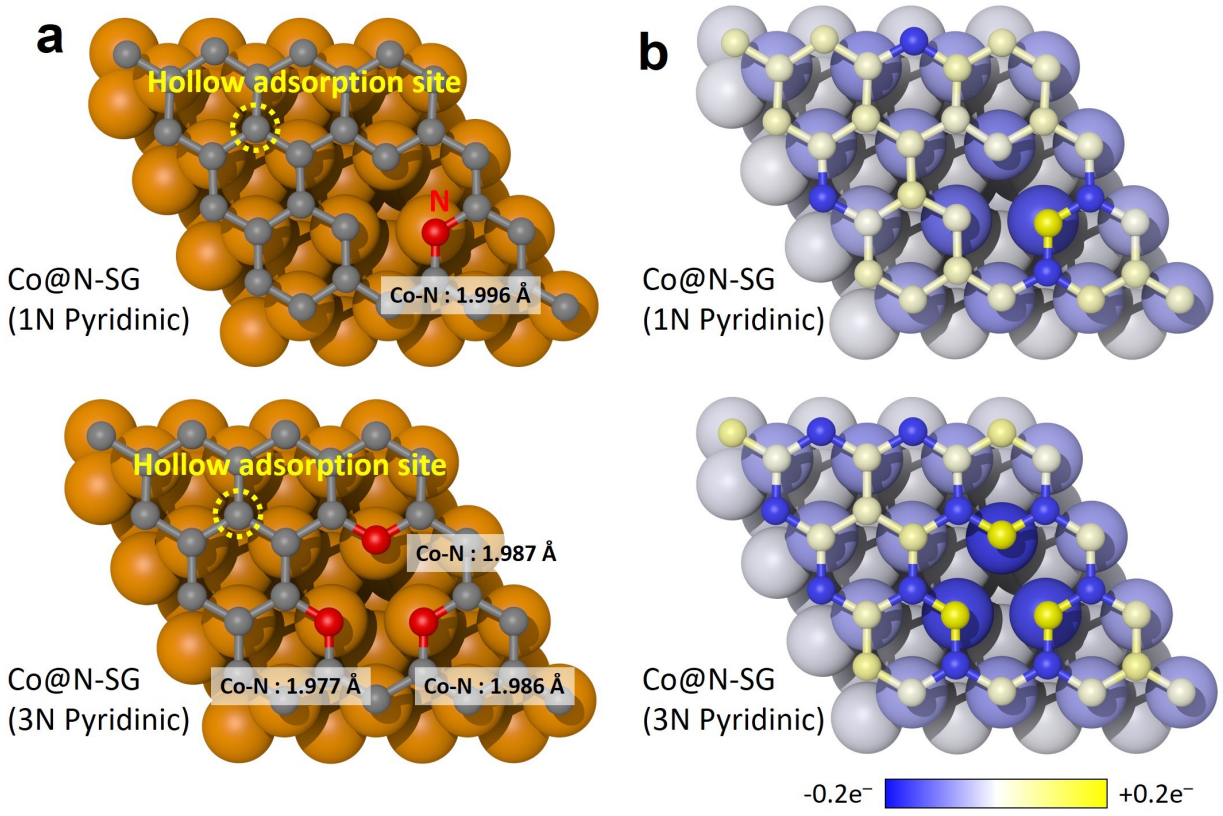

Fig. S20 Model systems of Co@N-SG and the charge distribution. a) Model systems of Co@N-SG (1N and 3N pyridinic). The orange, gray, and red spheres denote Co, C, and N atoms, respectively. The calculated Co-N bond distances are listed in the figure. b) Atomic charge density distributions on the Co@N-SG (1N and 3N pyridinic) without additional carbon defects. Blue and yellow contours indicate electron depletion and accumulation, respectively.

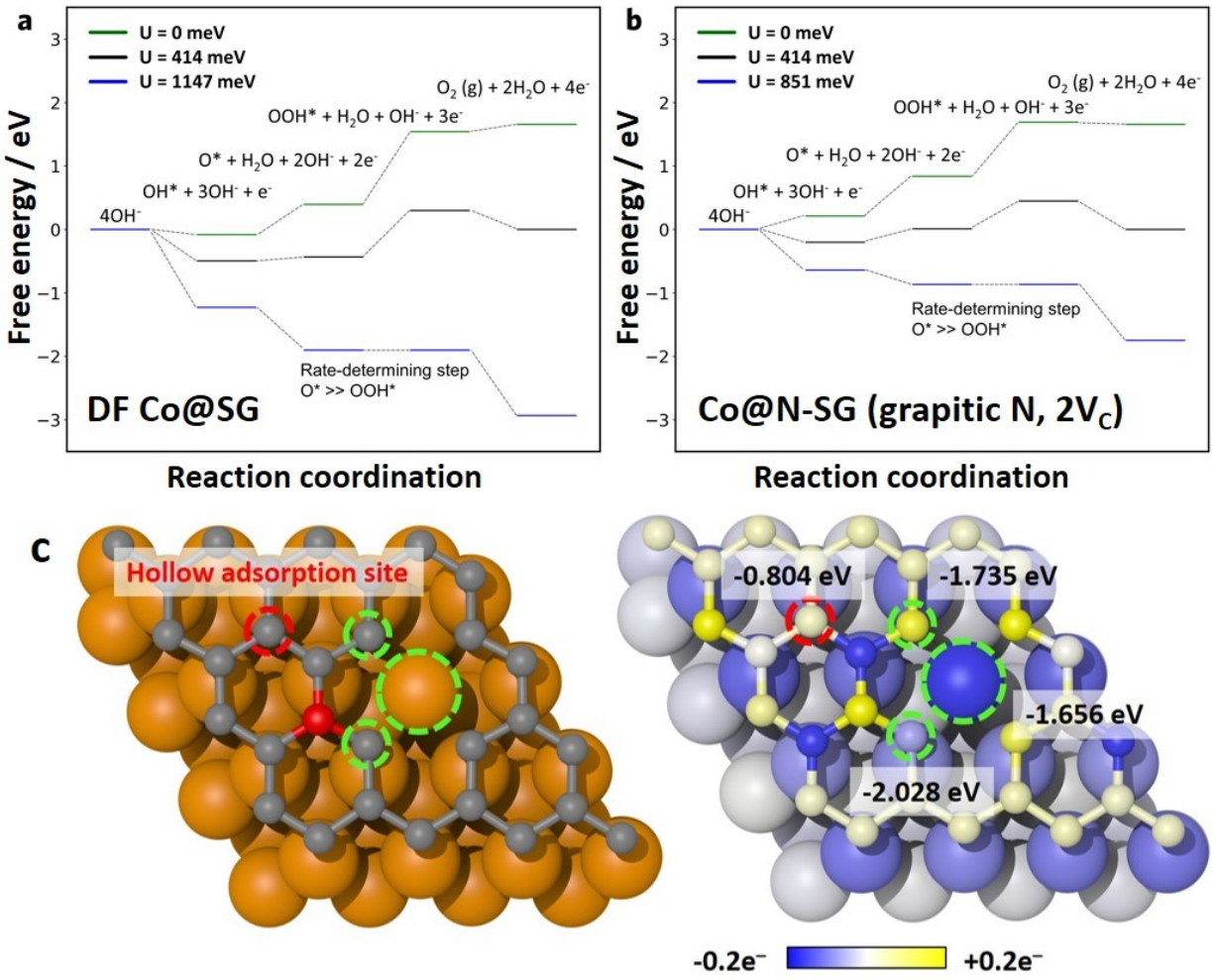

Fig. S21 OER free energy diagram and model system of Co@N-SG (graphitic N, $2V_C$) with the charge distribution. OER free energy diagram for a) DF Co@SG and b) Co@N-SG (graphitic N, $2V_C$) are presented. c) Calculated O atom adsorption energy for different C sites and Co site for Co@N-SG with graphitic N and 2Vc.

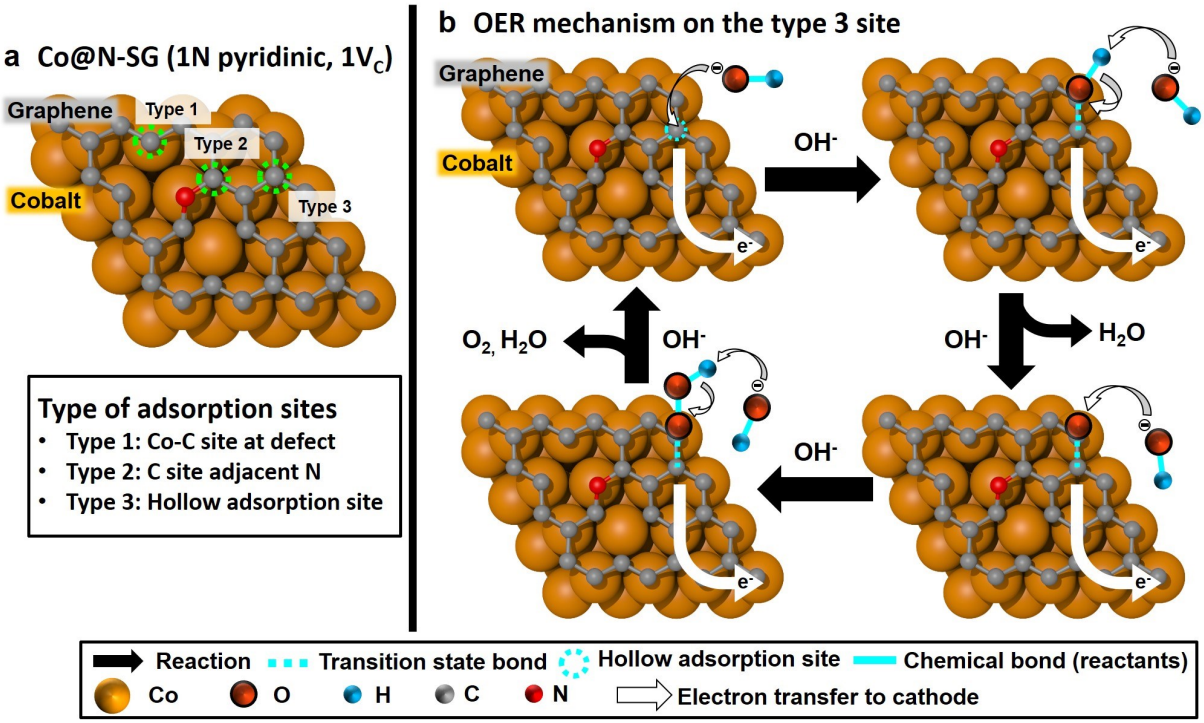

Fig. S22 Schematic diagram for proposed OER mechanism of Co@N-SG (1N pyridinic, 1V_C). a) Probable three different adsorption sites and b) OER mechanism on type 3 site (hollow adsorption site) of Co@N-SG (1N pyridinic, 1V_C).

References

1. G. Kresse, J. Furthmuller, *Phys. Rev. B*, 1996, **54**, 11169–11186.
2. J. P. Perdew, K. Burke, M. *Phys. Rev. Lett*., 1996, **77**, 3865.
3. P. E. Blochl, *Phys. Rev. B*, 1994, **50**, 17953–17979.
4. S. Grimme, J. Antony, S. Ehrlich, H. Krieg, *J. Chem. Phys*., 2010, **132**, 154104.
5. S. Liu, Z. Wang, S. Zhou, F. Yu, M. Yu, C. Y. Chiang, W. Zhou, J. Zhao, J. Qiu, *Adv. Mater*., 2017, **29**, 1700874.
6. Y. Noël, M. De La Pierre, C. M. Zicovich-Wilson, R. Orlando, R. Dovesi, *Phys. Chem. Chem. Phys*., 2014, **16**, 13390.
7. Y. Yao, Z. Xu, F. Cheng, W. Li, P. Cui, G. Xu, S. Xu, P. Wang, G. Sheng, Y. Yan, et al. *Energy Environ. Sci*., 2018, **11**, 407.
8. M. Tavakkoli, T. Kallio, O. Reynaud, A. G. Nasibulin, C. Johans, J. Sainio, H. Jiang, E. I. Kauppinen, K. Laasonen, *Angew. Chemie Int. Ed.*, 2015, **54**, 4535.
9. X. Cui, P. Ren, D. Deng, J. Deng, X. Bao, *Energy Environ. Sci*., 2016, **9**, 123.
10. A. Sivanantham, P. Ganesan, L. Estevez, B. P. McGrail, R. K. Motkuri, S. Shanmugam, *Adv. Energy Mater*., 2018, **8**, 1702838.
11. A. Aijaz, J. Masa, C. Rösler, W. Xia, P. Weide, A. J. R. Botz, R. A. Fischer, W. Schuhmann, M. Muhler, *Angew. Chem. Int. Ed*., 2016, **55**, 4087.
12. H. Guo, Q. Feng, J. Zhu, J. Xu, Q. Li, S. Liu, K. Xu, C. Zhang, T. Liu, *J. Mater. Chem. A*, 2019, **7**, 3664.
13. J. Chang, Y. Xiao, M. Xiao, J. Ge, C. Liu, W. Xing, *ACS Catal.*, 2015, **5**, 6874.
14. S. Mao, Z. Wen, T. Huang, Y. Hou, J. Chen, *Energy Environ. Sci*., 2014, **7**, 609.
15. B. Chen, X. He, F. Yin, H. Wang, D. J. Liu, R. Shi, J. Chen, H. Yin, *Adv. Funct. Mater*., 2017, **27**, 1700795.
16. X. Li, Z. Niu, J. Jiang, L. Ai, *J. Mater. Chem. A*, 2016, **4**, 3204.
17. G. H. Moon, M. Yu, C. K. Chan, H. Tüysüz, *Angew. Chem. Int. Ed.*, 2019, **58**, 3491.
18. B. Y. Xia, Y. Yan, N. Li, H. B. Wu, X. W. D. Lou, X. Wang, *Nat. Energy*, 2016, **1**, 15006.
19. N. Jiang, B. You, M. Sheng, Y. Sun, *Angew. Chemie - Int. Ed*., 2015, **54**, 6251.
20. T. Y. Ma, S. Dai, M. Jaroniec, S. Z. Qiao, *J. Am. Chem. Soc*., 2014, **136**, 13925.
21. Y. Liang, Y. Li, H. Wang, J. Zhou, J. Wang, T. Regier, H. Dai, *Nat. Mater*., 2011, **10**, 780.